HHS Public Access

Author manuscript

Mol Cancer Res. Author manuscript; available in PMC 2020 January 03.

Published in final edited form as:

Mol Cancer Res. 2019 April ; 17(4): 882–894. doi:10.1158/1541-7786.MCR-18-0990.

Serine Threonine Kinase 17A maintains the epithelial state in colorectal cancer cells

Sarah P. Short[1,2], **Joshua J. Thompson**[1,2], **Anthony J. Bilotta**[1], **Xi Chen**[3], **Frank L. Revetta**[4], **M. Kay Washington**[4], **Christopher S. Williams**[1,2,5,6,7]

[1]Department of Medicine, Division of Gastroenterology, Vanderbilt University Medical Center, Nashville, Tennessee, 37232, USA

[2]Program in Cancer Biology, Vanderbilt University, Nashville, Tennessee, 37232, USA

[3]Department of Public Health Sciences and the Sylvester Comprehensive Cancer Center, University of Miami Miller School of Medicine, Miami, Florida, USA.

[4]Department of Pathology, Microbiology, and Immunology, Vanderbilt University Medical Center, Nashville, Tennessee, 37232, USA

[5]Veterans Affairs Tennessee Valley Health Care System, Nashville, Tennessee, 37232, USA

[6]Center for Mucosal Inflammation and Cancer, Vanderbilt University Medical Center, Nashville, Tennessee, 37232, USA

[7]Vanderbilt Ingram Cancer Center, Nashville, Tennessee, 37232, USA

Abstract

Serine Threonine Kinase 17A (STK17A) is a ubiquitously expressed kinase originally identified as a regulator of apoptosis; however, whether it functionally contributes to colorectal cancer (CRC) has not been established. Here, we have analyzed STK17A in CRC and demonstrate decreased expression of STK17A in primary tumors which is further reduced in metastatic lesions, indicating a potential role in regulating the metastatic cascade. Interestingly, changes in STK17A expression did not modify proliferation, apoptosis, or sensitivity of CRC cell lines to treatment with the chemotherapeutic 5-fluorouracil. Instead, STK17A knockdown induced a robust mesenchymal phenotype consistent with the epithelial-mesenchymal transition, including spindle-like cell morphology, decreased expression of adherens junction proteins, and increased migration and invasion. Additionally, overexpression of STK17A decreased cell size and induced wide-spread membrane blebbing, a phenotype often associated with activation of cell contractility. Indeed, STK17A overexpressing cells displayed heighted phosphorylation of myosin light chain in a manner dependent on STK17A catalytic activity. Finally, patient-derived tumor organoid cultures were used to more accurately determine STK17A's effect in primary human tumor cells. Loss of STK17A induced morphological changes, decreased E-cadherin, increased invasion, and augmented organoid attachment on 2D substrates, all-together suggesting a more metastatic

Corresponding Author: Christopher S. Williams, M.D., Ph.D., Vanderbilt University Medical Center, 2231 Garland Ave, 1065D MRB-IV, Nashville, TN 37235-0654, (615) 322-3642; Fax (615) 343-6229, christopher.s.williams@vanderbilt.edu.

The authors declare no potential conflicts of interest.

phenotype. Collectively, these data indicate a novel role for STK17A in regulation of epithelial phenotypes and indicate its functional contribution to CRC invasion and metastasis.

Implications: Loss of serine threonine kinase 17A occurs in colorectal cancer metastasis, induces mesenchymal morphologies, and contributes to tumor cell invasion and migration in colorectal cancer.

Keywords

STK17A; DRAK1; colon cancer; epithelial-mesenchymal transition; tumor organoid

Introduction

In the United States, colorectal cancer (CRC) remains the third most commonly diagnosed cancer of men and women and the second leading cause of cancer-related mortalities (1). However, despite its prevalence, both CRC incidence and mortality have steadily declined over the past decades. This is in part due to increased screening and the ability to remove many early stage polyps and cancers before they progress to more advanced disease (2). Indeed, localized CRC is most commonly diagnosed, with a 5-year survival rate estimated at 90% (2). Unfortunately, for the approximately 20% of patients diagnosed with distant or metastatic disease, the 5-year survival rate is only about 14%. Thus, CRC mortality is primarily associated with metastatic disease (3).

Tumor metastasis is a sequential yet highly complicated process, involving tumor cell invasion into the surrounding microenvironment, intravasation into the local vasculature, arrest and extravasation, and establishment at a secondary site often primed to support tumor growth (4). While the biological mechanisms underlying the metastatic cascade remain poorly understood, the initial steps of tumor cell detachment from the primary tumor and local tissue invasion have often been compared to the developmental process of epithelial-mesenchymal transition (EMT), in which polarized epithelial cells acquire characteristics commonly associated with more migratory mesenchymal cells (5). For example, CRC cells located at the invasive tumor front often display EMT hallmarks, including loss of epithelial cadherin (E-cadherin), disrupted cellular polarity, upregulation of mesenchymal markers, altered morphology, and hypermigratory ability (6). However, the absolute requirement for EMT in metastasis is still controversial, and recent data suggests tumor cell invasion may be augmented when cells activate certain components of the EMT without inducing a fully mesenchymal state, which has been referred to as a “partial” or “hybrid” EMT (7,8).

Serine threonine kinase 17A (STK17A), also known as DAP kinase-related apoptosis-inducing protein kinase 1 (DRAK1), is a ubiquitously expressed kinase. It was originally noted to have a catalytic domain related to that of death-associated protein kinase (DAP) and observed to induce morphological changes associated with apoptosis, and therefore suggested to have a role in apoptotic signaling (9). Thus, in the years since its discovery, multiple studies have focused on its role in regulating cell death and chemotherapeutic resistance. For example, STK17A is induced by cisplatin in testicular cancer cells as a p53 target gene, while *STK17A* downregulation is observed in drug resistant subclones of MeWo melanoma cells (10,11). STK17A expression is upregulated following combined treatment

with the proteaseome inhibitor bortezomib and gemcitabine in gemcitabine-resistant pancreatic cancer cells (12). STK17A's roles in promoting apoptosis were thought to mediate the increased sensitivity observed by the combined therapies (12). Furthermore, depletion of *STK17A* in ovarian cancer cells by siRNA rendered them less sensitive to paclitaxel and carboplatin, while STK17A overexpression resulted in increased drug sensitivity (13). While not true for all tumor types analyzed to date, such as glioblastoma, overall results most commonly implicate STK17A as a tumor suppressor and regulator of chemotherapeutic resistance (14). However, its role has not been thoroughly evaluated in all cancers such as CRC.

However, while STK17A is known to be expressed in CRC cells and downregulated in oxaliplatin-resistant lines, whether STK17A functionally contributes to tumor growth, progression, or drug resistance in CRC is still unknown. Here, we report that STK17A is decreased in CRC as compared to normal human colon and is further decreased in metastatic lesions. Surprisingly, alteration of STK17A expression did not affect apoptosis or chemotherapeutic resistance in CRC. Instead, STK17A modulated epithelial/mesenchymal morphologies, migration, invasion, and expression of adherens junction (AJ) proteins in a manner consistent with a partial EMT. STK17A also increased cell contractility via phosphorylation of myosin light chain (MLC), and induced membrane blebbing consistent with previous reports of apoptotic morphologies (9). Importantly, many of these alterations were further confirmed in novel 3D "tumoroid" cultures isolated from human CRC tumors. Thus, this work identifies a previously unknown role for STK17A in maintaining epithelial phenotypes and indicate that loss of STK17A functionally contributes to CRC progression and metastasis.

Materials and methods

Cell culture and stable cell lines

HCT116 and SW480 cells were purchased from ATCC and authenticated by STR profiling prior to experimentation (ATCC). Cells were grown in McCoy's 5A medium (16600082, Gibco) supplemented with 10% fetal bovine serum, 100 U/ml penicillin, and 100 μg/ml streptomycin and verified to be mycoplasma free using the Universal Mycoplasma Detection Kit (30-1012K, ATCC). To generate STK17A knockdown lines, shRNA constructs (clones NM_004760.x-439s1c1 and NM_004760.x-1084s1c1) and a nontargeted scrambled control were purchased in the pLKO.1 lentiviral vector (Sigma-Aldrich). For overexpression, STK17A cDNA (SC117160, OriGene) was cloned into the pLEX-307 vector (a gift from Dr. David Root, 41392, Addgene), while GFP was cloned into the pLEX-307 vector to generate the pLEX-GFP control cell lines. The kinase dead K90A construct was generated from the pLEX-STK17A vector using the QuikChange II XL site-directed mutagenesis kit (200521, Agilent Technologies) using primers described in Supplemental Table 1.

Human RNA expression

STK17A levels were queried from the combined Moffitt Cancer Center/Vanderbilt Medical Center colon cancer expression array data set (GEO accession number GSE17538) as described previously (15,16). *STK17A* levels were also queried from Illumina HiSeq and

Illumina GA RNASeqV2 data in The Cancer Genome Atlas (TCGA) colon adenocarcinoma (COAD) data set (n = 264 CRC, 39 normal colon) (17). Normalized RSEM expression data were log2 transformed for visualization. *STK17A* expression was additionally correlated with patient survival in the Moffitt Cancer Center/Vanderbilt Medical Center colon cancer expression array data set, the TGCA COAD dataset, and with two independent *STK17A* probes in GSE39582, a large CRC expression study with 200 months of survival data (15-18). For human cell lines, *STK17A* expression data was queried from the Broad Institute Cancer Cell Line Encyclopedia RNA-sequencing and Affymetrix array mRNA public datasets (https://portals.broadinstitute.org/ccle)(19).

Immunohistochemistry

Matched primary tumor and metastasis arrays were generated by an experienced pathologist (M.K.W.). For STK17A analysis, five-micrometer sections from array blocks deparaffinized. Antigen retrieval was conducted by 20-minute incubation in a 104°C pressure cooker with citrate buffer (pH 6) followed by a 10-minute cool down. Slides were quenched with 0.03% H_2O_2 with sodium azide for 5 minutes, followed by incubation with serum-free protein block (X0909, Dako). After blocking, anti-STK17A primary antibody was added (ab111963, Abcam) and incubated for one hour. Staining was visualized with the Dako Envision+ HRP system and DAB. Staining intensity was quantified on a 0-4 scale by a blinded observer.

Immunofluorescent staining

HCT116 and SW480 cells plated on glass coverslips were fixed with paraformaldehyde, and permeabilized with Triton X prior to blocking in milk solution. Primary antibodies including anti-E-cadherin (610181, BD Biosciences), anti-α-catenin (C2081, Sigma-Aldrich), anti-ZO-1 (617300, ThermoFisher), and anti-STK17A (ab111963, Abcam) were incubated for 30 minutes in milk solution. After washing, species-specific Alexa Fluor 488 or 568 secondary antibodies (Life Technologies) or ActinGreen/ActinRed ReadyProbes (Life Technologies) were applied for 30 minutes. Coverslips were mounted on glass slides with ProLong Gold antifade reagent with DAPI (P36931, Life Technologies) and visualized with a Nikon Eclipse E800 microscope and Zyla SCMOS camera. Images were processed in Nikon NIS-Elements Basic Research software. For tumoroid staining, glass coverslips were coated with a 1:1 mixture of media and growth factor reduced Matrigel (356231, Corning) prior to cell seeding.

Morphological Analysis

Cells were plated on glass coverslips and stained with ActinGreen/ActinRed and DAPI. Images collected with NIS: Basic Research software were exported and cell morphologies were measured using CellProfiler software and associated modules to measure cell size and shape (20).

Western Blot Analysis

Cells were lysed in RIPA buffer, phosphatase inhibitor cocktail 2 (P5726, Sigma Alrich), phosphatase inhibitor cocktail 3 (P0044, Sigma-Aldrich), protease inhibitor (P8340, Sigma-Aldrich), and 2X Laemmli buffer and boiled for 10 minutes before analysis by SDS-PAGE

electrophoresis. Membranes were blocked using Odyssey blocking buffer (LI-COR) and then blotted with anti-E-cadherin (610181, BD Biosciences), anti-ZO-1 (617300, Life Technologies), anti-α-catenin (C2081, Sigma-Aldrich), anti-STK17A (ab111963, Abcam), anti-STK17B (ab56506, Abcam), anti-GAPDH (5174S, Cell Signaling Technologies), anti-β-tubulin (Vanderbilt Antibody and Protein Resource), anti-myosin light chain 2 (8505S, Cell Signaling Technologies), or anti-phospho-myosin light chain 2 (3674S, Cell Signaling Technologies) in Odyssey blocking buffer overnight. LI-COR secondary antibodies were used at 1:20,000 dilution and incubated for 1 hour at room temperature. Quantification of western blot band intensity was conducted using LI-COR Image Studio.

RNA isolation and quantitative real-time PCR

RNA was isolated using the RNeasy Mini Kit (74106, Qiagen) with on column DNase treatment. cDNA was synthesized using the qScript cDNA SuperMix (95048, Quantabio) from 2 μg of total RNA. qPCR reactions were run using PerfeCTa SYBR Green SuperMix ROX (95055, Quantabio) and primers designated in Supplemental Table 1. Each sample was run in triplicate and target gene expression was analyzed using the delta–delta Ct method and normalized to *GAPDH.*

Viability assays

2.5×10^3 cells were seeded into a 96 well plate. For proliferation, cell numbers were analyzed using the CellTiter-Glo 2.0 Luminescent Cell Viability Assay (G9241, Promega) according to manufacturer's instructions. For chemotherapeutic sensitivity, 5-fluorouricil (5-FU, F6627, Sigma-Aldrich) was dissolved in media and diluted as described. 24 hours post plating and directly prior to 5-FU treatment, baseline cell viability was determined using the CellTiter-Blue Cell Viability Assay (G8080, Promega) according to manufacturer's instructions. Viability was again measured 72 hours post treatment, and the results of each well were divided by the baseline reading and normalized to untreated samples. For all viability measurements, samples were run in triplicate and background was subtracted as calculated by measuring media only control wells. Readings were obtained using the GloMax Discover plate reader (Promega) and manufacturer-designated programs.

Human tumor organoids

Deidentified human colorectal tumor tissue samples were collected at Vanderbilt University Medical Center and provided by the NCI Cooperative Human Tissue Network (CHTN) in accordance with the Vanderbilt Institutional Review Board. Other investigators may have received specimens from the same tissue specimens. Known clinical features are described in Supplemental Table 2. Tumor organoids were established according to previously published protocols (21). Briefly, minced tumor tissue was incubated in digestion buffer (Advanced DMEM F12, Gibco; 10% FBS; 100 U/ml penicillin; 100 μg/ml streptomycin; 0.125mg/ml Dispase II, Roche; 0.1mg/ml collagenase XI; Sigma-Aldrich) for 1 hour at 37°C. Following digestion, the supernatant containing digested tumor fragments was collected, washed, and suspended in Matrigel (356231, Corning). After polymerization, Matrigel plugs were overlaid with human organoid media as described in Supplemental Table 3.

To generate stable tumor organoid lines, lentivirus was generated and concentrated by spinning at 8000rpm overnight. Organoids were collected and digested in TrypLE Express (12604039, Gibco) prior to suspension in lentivirus-containing media supplemented with 8μg/ml polybrene (Millipore) and 10μM Y-27632 (125410, Tocris). Organoids were spinoculated for 1 hour at 600g followed by incubation for 6 hours at 37°C. After infection, cells were resuspended in Matrigel and overlaid with human culture media supplemented with 10μM Y-27632.

Migration and invasion assays

Migration assays using magnetically attachable stencils (MAts) were conducted as described in previously published protocols (22). Briefly, MAts were attached to a 6-well plate using magnets and 2×10^6 cells were seeded into each MAts-containing well. 24 hours post-plating, cells were refed with McCoy's 5A medium containing 0.5% FBS and serum starved overnight. The next day, cells were refed with complete media with 10% FBS and the stencils removed. Voids created by MAts removal were imaged at timepoints noted.

For transwell migration assays, HCT116 or SW480 cells were serum starved overnight. The following day, 5×10^4 cells were seeded into the top of 8μm pore, 24-well transwell inserts (662635, Greiner Bio) in 0.5% FBS-containing media while the outer well was filled with 10% FBS-containing media. Cells were allowed to migrate for 72 hours prior to fixation and staining using the Hema 3 staining kit (23-123869, Fisher Scientific). Invasion assays were done similarly using BioCoat™ Matrigel Invasion Chambers (354483, Corning) according to manufacturer's instructions. For invasion assays using human tumor organoids, organoids were dissociated and 5×10^4 cells were seeded into the top of prepared BioCoat™ Matrigel Invasion Chambers in reduced media containing Advanced DMEM F12, 20% R-spondin conditioned media, 10% Noggin conditioned media (23), 1x B27, 1x N2, 1x Glutamax, 1mM HEPES, 100 U/ml penicillin, and 100 μg/ml streptomycin. Complete human organoid media was placed in outer well. Cells were allowed to invade for 96 hours prior to fixing, staining, and analyzing as described above. Quantification for all assays was done using ImageJ software.

Soft agar assays

To analyze anchorage-independent growth, 1×10^3 cells were suspended in 0.33% agarose (A20090500, RPI) in complete media in a 12-well dish and overlaid with complete media (24,25). Colonies were counted and imaged after 10 days. Colony size quantification (area in pixels) was performed using ImageJ software.

2D tumor organoid growth

To analyze ability of tumor organoids to attach and grow as 2D cultures, organoids were collected and dissociated with TrpLE express and 2×10^5 cells were seeded in human organoid media into a 6-well uncoated tissue culture plate. After 2 days, wells were imaged for analysis of area covered using ImageJ software (5-6 images per condition/experiment). Afterward, cells were collected for cell viability analysis by CellTiter-Glo 2.0 Luminescent Cell Viability Assay (G9241, Promega). CellTiter-Glo readings were normalized to cell

samples taken directly post plating. For blebbistatin treatments, tumor organoid cells were plated with 50μM blebbistatin (B0560, Sigma-Aldrich) or DMSO alone.

Statistical methods

Statistical analysis comparing two or more groups was performed in Graphpad Prism Software using unpaired Student's t-test or one-way ANOVA with Tukey's multiple comparisons post-test, respectively. Outliers were identified and removed using the Robust regression and Outlier removal (ROUT) method. For mRNA analysis, Wilcoxon rank sum test with continuity correction was used to compare each CRC stage to normal colon. For all studies, error is represented by standard error of the mean and $P<0.05$ is considered significant.

Results

STK17A is expressed in the colon and downregulated in CRC

We initially assessed *STK17A* levels in CRC in the Moffitt/Vanderbilt-Ingram Cancer Center CRC expression array dataset (Fig. 1A)(15,16). In line with a role as a tumor suppressor, *STK17A* was expressed in the colon and downregulated in adenomas as well as in all stages of CRC. Similar results were obtained querying RNA-sequencing data from The Cancer Genome Atlas (TCGA) colon adenocarcinoma data set (17). These results also demonstrate reduced *STK17A* expression in all stages of CRC, including early stage lesions (Normal vs. CRC, $P<0.0001$, Fig. 1B). However, *STK17A* mRNA expression was not associated with patient survival in any datasets queried (Supplemental Fig. 1)(15-18).

We next analyzed STK17A protein expression by immunohistochemistry. Here, we observed STK17A expression in the colon was predominantly localized to the differentiated colonocytes, while expression was reduced in the colonic crypts (Fig. 1C, left). In agreement with the mRNA analysis, protein expression was also decreased in CRC samples (Fig. 1C, right). Interestingly, despite equivalent changes in *STK17A* mRNA expression in both low and high stage tumors, a microarray of matched primary CRC and liver metastases indicated that STK17A protein levels were preferentially decreased in metastases (Fig. 1D). Samples from CRC liver metastases had less intense staining for STK17A than that observed in primary tumors (1.8 ± 0.1 vs. 1.2 ± 0.2, $P<0.05$). To further investigate whether *STK17A* levels were decreased in metastasis, mRNA levels were queried from RNA-sequencing and Affymetrix expression array datasets compiled by the Broad Institute's Cancer Cell Line Encyclopedia for the SW480 and SW620 colon cancer cell lines (19). Interestingly, SW620 cells, which were established from a metastatic tumor, showed decreased *STK17A* mRNA expression as compared to the SW480 line, derived from a primary tumor in the same patient (Fig. 1E)(26). Furthermore, expression in common CRC cell lines derived from primary tumors (SW480, HCT116, Caco-2, DLD1, RKO, HCT-8) was compared to available metastatic-derived lines (SW620, COLO 205, COLO 201, LoVo, SNU-C1), which again illustrated decreased expression in metastatic tumor cells (7.4 ± 0.3 vs. 6.4 ± 0.3, $P<0.05$). As STK17A was reduced in CRC and further reduced in metastases, we hypothesized that loss of STK17A may functionally contribute to tumor progression and metastasis in CRC.

Loss of STK17A induces mesenchymal phenotypes in CRC cells

To determine whether STK17A downregulation augments pro-metastatic phenotypes, we knocked down (KD) *STK17A* by shRNA in CRC cell lines. Two cell lines were chosen, HCT116 and SW480, as both cell lines are established from primary human colon tumors (26,27). Decreased levels of *STK17A* mRNA (Fig. 2A, left) and protein (Fig. 2A, right) were observed in the stable *STK17A* shRNA KD lines. Further, alteration of STK17A expression did not affect levels of the STK17A family member, STK17B. Interestingly, *STK17A* KD induced a robust mesenchymal phenotype in both cell lines and *STK17A* KD cells demonstrated elongated, spindle morphology as compared to control cells expressing a nontargeted, scrambled shRNA sequence (Fig. 2B & 2C). This change in morphology was further confirmed by quantification using CellProfiler software (Fig. 2D)(20). HCT116 *STK17A* KD cells consistently demonstrated increased length (1±0.04 vs. 2.4±0.06, $P<0.0001$) and perimeter (1±0.03 vs. 2±0.08, $P<0.0001$) while the form factor, a surrogate for cell roundness, was significantly decreased (1±0.03 vs. 0.48±0.02, $P<0.0001$) as compared to control cells. Further, a consistent but more modest phenotype was observed in HCT116 cells using a different, less efficient shRNA construct (shSTK17A #2) which yielded a much lower degree of STK17A KD, suggesting a dose-dependent phenotypic effect (Supplemental Fig. 2). Together, these results indicate STK17A maintains an epithelial phenotype and its loss induces mesenchymal changes consistent with EMT.

Downregulation of cell-cell adhesion molecules, particularly E-cadherin, is a hallmark of EMT and key contributor to loss of the epithelial phenotype. To next determine whether *STK17A* loss induced changes in cell-cell adhesion proteins, HCT116 and SW480 KD cells were analyzed by immunohistochemistry. Here, we observed decreased staining for E-cadherin and α-catenin, an E-cadherin binding partner which connects the AJ to the cytoskeleton, in both HCT116 (Fig. 3A) and SW480 cell lines (Fig. 3B)(28). The decrease in E-cadherin and α-catenin was further confirmed by western blot (WB), indicating that the attenuated staining was due to reduced protein levels and not abnormal protein localization (Fig. 3C). On the other hand, expression of proteins associated with the tight junction (TJ), such as ZO-1, were relatively unchanged by both staining and WB analysis (Fig. 3C & 3D). Because EMT alterations are often mediated at the transcriptional level (29), we next assessed mRNA levels of E-cadherin (*CDH1*) and Vimentin (*VIM*), an intermediate filament specifically expressed in mesenchymal cells and considered a canonical marker of EMT (30). Interestingly, *CDH1* expression was unchanged in HCT116 *STK17A* KD cells, although *VIM* was highly upregulated (Fig. 3E). Conversely, *VIM* expression was unchanged in SW480 KD cells while *CDH1* was downregulated. Thus, each cell line appears to induce a “partial EMT” which likely drives the mesenchymal phenotype observed after *STK17A* loss.

STK17A modulates cell migration and invasion

Developmentally, epithelial cells induce EMT to allow migration within the embryo while, in cancer, EMT is associated with cell invasion and metastasis (5,30). Therefore, we hypothesized that the mesenchymal morphology observed after *STK17A* KD would augment cell migration. We first tested this hypothesis using magnetically attachable stencils (MAts) to create a well-defined “wound” within the cell monolayer and migration into the

cell-free area was quantified at various timepoints post stencil removal (Fig. 4A)(22). Decreased wound area was observed at all timepoints in *STK17A* KD cells (16hr: 66±0.8% vs. 55.5±0.8%; 24hr: 47.4±3.1% vs. 32.7±4.6%; 48hr: 19.5±4.5% vs. 2.8±1.8%), suggestive of enhanced migration. Increased wound closure rates in this model were not due to changes in cell proliferation (Supplemental Fig. 3). Migration was also assessed by transwell migration assay and again indicated hypermigratory abilities in both *STK17A* KD lines (Scr.: 1±0.08; shSTK17A #1: 3.9±0.4, $P<0.0001$ vs Scr.; shSTK17A #2: 2.3±0.4, $P<0.01$ vs. Scr. and $P<0.001$ vs. shSTK17A #1, Fig. 4B). The smaller increase observed in the shSTK17A #2 line again suggests the degree of STK17A-driven phenotypes are dose-dependent (Fig. 4B). Additionally, transient expression of a non-sh targeted STK17A construct in the stable *STK17A* KD cells attenuated the migration increase induced by *STK17A* KD (Scr.: 1±0.1; shSTK17A: 13.2±0.1, $P<0.0001$ vs Scr.; V5-STK17A: 9.3±0.2, $P<0.0001$ vs. WT and shSTK17A, Fig. 4C), demonstrating an on-target effect of *STK17A* KD. Cell invasion was also increased by STK17A loss, as measured using modified transwell inserts coated with Matrigel (1±0.2 vs. 4.8±0.6, $P<0.0001$, Fig. 4D). Together, these data indicate that the changes in morphology and AJ protein expression in *STK17A* KD cells functionally contribute to increased cell migration and invasion in CRC.

STK17A overexpression augments epithelial phenotypes

As a mesenchymal phenotype was observed with STK17A loss, we next aimed to determine whether increased STK17A expression augmented epithelial phenotypes or influenced cell morphology in CRC cells and STK17A (pLEX-STK17A) was stably expressed in HCT116 and SW480 cells (Fig. 5A). Interestingly, while a more mesenchymal, spindle-shaped morphology was observed in *STK17A* KD cells, HCT116 cells overexpressing STK17A appeared smaller and rounder than GFP-expressing control cells (pLEX-GFP, Fig. 5B). Quantification using CellProfiler indicated pLEX-STK17A cells indeed had decreased perimeter (1±0.02 vs. 0.8±0.01, $P<0.0001$) and increased form factor (1±0.02 vs. 1.3±0.02, $P<0.0001$) over that observed in control cells (Fig. 5C). Next, we assessed expression of AJ and TJ proteins by immunohistochemistry. In contrast to shSTK17A cells which lost expression of AJ-associated proteins, ectopic *STK17A* expression increased staining intensity for α-catenin, E-cadherin, and ZO-1 (Fig. 5D). Interestingly, protein levels as measured by WB were not greatly altered by *STK17A* overexpression, suggesting the increased staining intensity is likely due to increased membrane recruitment of junctional proteins or smaller cell size (Fig. 5E). Overall, these data suggest that STK17A induces epithelial phenotypes in CRC cells. To more rigorously test this hypothesis, we analyzed anchorage independent growth in HCT116 and SW480 STK17A overexpressing cells by soft agar assay. Importantly, anchorage independent growth is a characteristic of EMT in vitro and this ability is often lost in mesenchymal-to-epithelial transition(31). Here, we observed that overexpression of STK17A abrogated anchorage independent growth in both HCT116 and SW480 cell lines, and overexpressing cells yielded fewer colonies (HCT116: 1±0.04 vs. 0.55±0.09, $P<0.01$; SW480: 1±0.02 vs. 0.22±0.02, $P<0.0001$) and smaller colony size (HCT116: $4.7\times10^4\pm6.1\times10^3$ vs. $1\times10^4\pm1.5\times10^3$ pixels, $P<0.0001$; SW480: $5.4\times10^3\pm5.8\times10^2$ vs. $1.8\times10^3\pm1.7\times10^2$ pixels, $P<0.0001$) (Fig. 5F). Collectively, these data indicate that STK17A is a positive regulator of epithelial phenotypes in CRC cells.

STK17A induces cell contractility and phosphorylation of myosin light chain

At its initial discovery, STK17A was thought to regulate apoptotic signaling due to its ability to induce membrane blebbing, often considered a pre-apoptotic event, and is regulated by cytoskeletal dynamics (9,32). Interestingly, we observed STK17A overexpression in SW480 to also result in prominent membrane blebbing (Fig. 6A). However, this did not result in apoptosis, as overexpression of STK17A had no effect on cell viability in either HCT116 or SW480 line (Fig. 6B), nor did it sensitize cells to treatment with 5-FU, an agent known to induce apoptosis in CRC cells (Fig. 6C). Similarly, no effect on viability or chemotherapeutic sensitivity were observed following *STK17A* KD (Supplemental Figure. 3).

Membrane blebbing can also be a transient, non-apoptotic event driven by aberrant cell contraction. Often, this is associated with activation of the cytoskeletal protein, non-muscle myosin II, by phosphorylation of its regulatory light chain (myosin light chain, MLC) at serine 19 (33,34). To next determine whether STK17A-dependent membrane blebbing was dependent on myosin-mediated cell contractility, cells were treated with blebbistatin, a small molecule which inhibits myosin II contraction and has been shown to decrease membrane blebbing and induce cell elongation and mesenchymal morphology (35,36). Indeed, pLEX-STK17A cells treated with 100μm blebbistatin demonstrated loss of membrane blebbing and restoration of cell-cell contract (Fig. 6D). Further, increased MLC activation and phosphorylation was observed by WB in both HCT116 and SW480 cell lines (Fig. 6E). As STK17A is a kinase previously shown to phosphorylate MLC using purified proteins, we next hypothesized that STK17A's effect on MLC phosphorylation would be dependent on its kinase domain (9). Indeed, expression of the kinase-dead K90A construct abolished its effect on membrane blebbing (Fig. 6F) and MLC phosphorylation (Fig. 6G). In contrast to *STK17A* KD, STK17A overexpression decreased cell migration (1±0.03 vs. 0.6±0.04, $P<0.05$), and this effect was likewise dependent on kinase activity (1.1±0.2, n.s. vs. GFP, Fig. 6H) (9). Together, these data indicate that STK17A may regulate cell morphology and migration by increasing contraction via MLC phosphorylation.

STK17A regulates epithelial phenotypes in primary human tumor cells

To determine the pathophysiologic translation of these observations to CRC, we next utilized a 3D culture system of primary human CRC samples. The 3D tumor organoid approach has been increasingly used in recent years to model tumor cell behavior and therapeutic response, as organoids have been shown to more closely maintain morphology, histology, and cell heterogeneity than 2D cell lines (21,37). Human tumor organoids were established from primary CRC tumors (Supplemental Table 2), and 3 independent lines expressing detectable levels of STK17A (referred to as HTO1, HTO2, and HTO3) were selected for *STK17A* KD (Supplemental Figs. 4 & 5). Interestingly, while *STK17A* KD resulted in little phenotypic change in HTO2 (Supplemental Fig. 4), HTO1 *STK17A* KD organoids often appeared to invade through the Matrigel™ plug and adhere to the bottom of the tissue culture dish, resulting in an elongated and flattened morphology reminiscent of that observed in HCT116 and SW480 shSTK17A cells (Fig. 7A). Furthermore, immunofluorescent staining of HTO1 cells plated on coverslips for E-cadherin and α-catenin indicated that *STK17A* KD led to decreased staining for AJ proteins as seen in

standard tissue culture cell lines (Fig. 7B). To directly test whether *STK17A* KD induced functional changes which could contribute to tumor invasion and metastasis, HTO lines were dissociated and plated into Matrigel-coated transwell inserts to assess invasive potential. Even without an induction of mesenchymal morphology in HTO2, both HTO1 and HTO2 demonstrated increased invasion following *STK17A* KD, (HTO1: 5.8±1.6 vs. 29.7±3.2 cells per field, $P<0.0001$; HTO2: 3.9±1.2 vs. 12.3±2 cells per field, $P<0.01$)(Fig. 7C). Furthermore, HTO1 and HTO2 lines both showed a similar induction of the EMT-associated gene *VIM* by qPCR analysis (HTO1: 1±0.09 vs. 2.2±0.3, $P<0.05$; HTO2: 1±0.03 vs. 7±0.06, $P<0.0001$)(Fig. 7D). Together, these data indicate that STK17A regulates invasion and epithelial phenotypes in primary CRC tumor cells. However, it is worth noting that no phenotypic changes were induced in the HTO3 line (Supplemental Figure 5), likely due to inter-tumor heterogeneity and highlighting the wide variation of primary tumor phenotypes that are preserved utilizing 3D culture methods.

In addition to invasion, the morphological changes in HTO1 indicate that STK17A KD may increase cell adherence and spreading independent of basement substrate. Interestingly, the process of cell spreading is regulated in part by activity of RhoA and myosin light chain, and deactivation of these pathways increases cell spreading (38). As STK17A was observed to positively regulate MLC activity in HCT116 and SW480 cells (Fig. 6), we next directly tested whether STK17A affected cell attachment and cell spreading by dissociating organoid lines with and without *STK17A* KD and plating 2D in tissue culture plates (Fig. 7E & 7F). Indeed, loss of *STK17A* increased attachment in both lines (HTO1: 1±0.03 vs. 2.3±0.3, $P<0.01$; HTO2: 1±0.1 vs. 4±0.4, $P<0.001$). Importantly, treatment with blebbistatin to inhibit non-muscle myosin II increased cell spreading in control cells to levels seen with *STK17A* KD (1±0.04 vs. 4.2±0.6, $P<0.01$, Fig. 7F), indicating that alterations in MLC activity likely contribute to this process (35). Taken together, these results indicate that loss of STK17A regulates cell contractility and epithelial morphologies in human tumor cells and that its loss may functionally contribute to CRC tumor cell invasion and metastasis.

Discussion

The studies herein are the first to determine whether STK17A functionally contributes to CRC tumor growth and progression. While a previous study has reported STK17A expression in a single CRC cell line, this lacked functional characterization (39). Here, we identify a novel role for STK17A in modulation of epithelial and mesenchymal morphologies, cell-cell junctions, and contractility. Functionally, these changes augment cell migration and invasion in the setting of STK17A loss and indicate that STK17A expression is physiologically relevant to tumor biology and metastasis.

While STK17A's effect on tumor biology is relatively uncharacterized, the available studies suggest the role of STK17A may be highly specific to tumor type, supported by our observations. Indeed, STK17A has been reported to act as a tumor suppressor in testicular and ovarian cancer cells, and its overexpression decreased cell proliferation and induced greater sensitivity to chemotherapeutic agents (10,12,13). These roles are likely modulated by p53-dependent signaling mechanisms, as STK17A has been identified both as a p53 target gene as well as a p53 binding partner (10,40,41). However, our results were unlike

these studies in that we identified no alteration in CRC cell proliferation, apoptosis, and/or chemotherapeutic drug resistance induced by *STK17A* downregulation or overexpression. Interestingly, in other tumor types, STK17A is thought to act as a tumor promoter. Its overexpression has been proposed as a biomarker of more advanced disease in cervical cancer, and STK17A promotes both cell proliferation and survival in glioblastomas (14,42). Together, these indicate a highly relevant cancer-type dependency of STK17A function, which is not an uncommon phenomenon in cancer biology. For example, components of the Notch signaling cascade, such as the receptor NOTCH1, have been ascribed both oncogenic and tumor suppressive roles. A translocation resulting in a dominant active form of NOTCH1 is sufficient to induce lymphoblastic leukemia in mouse models, although *Notch1*$^{-/-}$ mice are more susceptible to tumor development in both skin and brain tumor models (43). We further observed that in CRC, *STK17A* loss did not affect all human tumor organoids equivalently, as augmentation of aggressive phenotypes, such as invasion, induction of mesenchymal markers, and substrate-independent growth, was observed in HTO1 and HTO2, while HTO3 was unaffected. This difference in effect is perhaps not surprising, given the considerable genetic variance between primary tumors. However, it was notable that the unresponsive HTO3 line was established from a low-grade tumor, while HTO1 and HTO2 were established from high grade tumors (Supplemental Table 2). Thus, STK17A loss may disproportionately affect higher grade tumors and serve as a final “hit” to induce CRC metastasis.

Interestingly, both STK17A and its family member, STK17B, have been previously shown to contribute to oncogenic growth of head and neck cancers by inhibiting the transforming growth factor β (TGF-β) pathway (44,45). Mechanistically, both proteins differentially inhibit SMAD3, with STK17A found to directly bind to SMAD3 and block its translocation into the nucleus and interaction with Smad4. In this manner, STK17A overexpression circumvents TGF-β-mediated growth inhibition. However, in addition to growth inhibition, the TGF-β pathway is a key regulator of EMT, suggesting that some effects of STK17A on cell migration and invasion may be due to interaction with the TGF-β pathway (46). However, it is important to note that components of the TGF-β pathway are common targets of inactivating mutations in CRC (47,48). Indeed, both HCT116 and SW480 cells have mutational inactivation of key TGF-β pathway components, as HCT116 cells have inactivating mutations in *TGFβR2* while SW480 cells have complete loss of *SMAD4* (49,50). Further investigation into the role of STK17B has also indicated that its effect on TGF-β activity does not extend to all cell types, as no regulation of TGF-β activity was determined in T-cells (51). Thus, while STK17A and/or STK17B may contribute to TGF-β-dependent signaling, this mechanism is unlikely to be relevant to CRC.

Instead, the effect of STK17A expression observed in these studies appear mostly likely due to a role in cell contractility and regulation of myosin light chain. Interestingly, the first studies describing STK17A noted that STK17A expression induced the apoptosis-associated morphology of membrane blebbing, which is also known to be induced by aberrant activation of RhoA and MLC phosphorylation (9,32). Importantly, MLC is one of the very few targets of STK17A phosphorylation identified to-date, as STK17A has been determined phosphorylate MLC as an exogenous substrate (9). However, these studies herein are the first to show STK17A-dependent modulation of MLC phosphorylation in an *in vitro* setting

or its relevance to cellular phenotypes. We further show that this effect is dependent on the kinase domain of STK17A, which suggests direct regulation of MLC. Interestingly, STK17A's effect on cell contractility may further its contribution to metastatic spread by regulation of anoikis, a type of cell death triggered by cell detachment and necessary to survival in the lymphatic and vascular systems (52). Importantly, anoikis is thought to be regulated in party by aberrant cell contractility, as viability of detached cells can be increased by inhibition of RhoA downstream effectors, such as ROCK1 or myosin (53). In line with this role, overexpression of STK17A attenuated anchorage-independent growth in soft agar. Thus, STK17A expression likely regulates multiple points of the metastatic cascade.

Here, using multiple cell lines complemented by novel tumor organoid cultures, the data herein is the first to describe a functional role for STK17A in CRC progression. Furthermore, these data indicate a previously unknown role for STK17A in EMT and maintaining the epithelial state, and suggest that STK17A may influence tumor invasion, progression, and metastasis in CRC. As the majority of CRC-associated deaths are due to metastatic disease, pathways which contribute to cell invasion and migration are of the utmost interest. These data further our understanding of molecular drivers of EMT as well as describe novel roles for the STK17A kinase.

Supplementary Material

Refer to Web version on PubMed Central for supplementary material.

Acknowledgements

We thank all members of the Williams laboratory for thoughtful discussions about this research project. Additionally, we would like to thank the Vanderbilt Translational Pathology Shared Resource core for assistance with slide preparation and H&E staining, as well as the Vanderbilt Cooperative Human Tissue Network for tissue procurement. This work was supported by National Institutes of Health R01DK080221 to CSW, F32DK108492 to SPS, F30DK111107 to JJT, and P30DK058404 to MKW, and the Office of Medical Research, Department of Veterans Affairs I01BX001426 to CSW. This project was also supported by CTSA award No. UL1 TR002243 from the National Center for Advancing Translational Sciences. Its contents are solely the responsibility of the authors and do not necessarily represent official views of the National Center for Advancing Translational Sciences or the National Institutes of Health.

Financial support includes National Institutes of Health (UL1 TR002243; R01 DK080221 to C.S.W.; F32 DK108492 to S.P.S.; F30 DK111107 to J.J.T); Office of Medical Research, Department of Veterans Affairs (I01BX001426 to C.W.)

References

1. Siegel RL, Miller KD, Jemal A. Cancer Statistics, 2017. CA Cancer J Clin 2017;67:7–30 [PubMed: 28055103]
2. Siegel RL, Miller KD, Fedewa SA, Ahnen DJ, Meester RGS, Barzi A, et al. Colorectal cancer statistics, 2017. CA Cancer J Clin 2017;67:177–93 [PubMed: 28248415]
3. Zacharakis M, Xynos ID, Lazaris A, Smaro T, Kosmas C, Dokou A, et al. Predictors of survival in stage IV metastatic colorectal cancer. Anticancer Res 2010;30:653–60 [PubMed: 20332485]
4. Lambert AW, Pattabiraman DR, Weinberg RA. Emerging Biological Principles of Metastasis. Cell 2017;168:670–91 [PubMed: 28187288]
5. Chaffer CL, Weinberg RA. A perspective on cancer cell metastasis. Science 2011;331:1559–64 [PubMed: 21436443]

6. Brabletz T, Jung A, Spaderna S, Hlubek F, Kirchner T. Opinion: migrating cancer stem cells - an integrated concept of malignant tumour progression. Nat Rev Cancer 2005;5:744–9 [PubMed: 16148886]
7. Li W, Kang Y. Probing the Fifty Shades of EMT in Metastasis. Trends Cancer 2016;2:65–7 [PubMed: 27042694]
8. Jolly MK, Boareto M, Huang B, Jia D, Lu M, Ben-Jacob E, et al. Implications of the Hybrid Epithelial/Mesenchymal Phenotype in Metastasis. Front Oncol 2015;5:155 [PubMed: 26258068]
9. Sanjo H, Kawai T, Akira S. DRAKs, novel serine/threonine kinases related to death-associated protein kinase that trigger apoptosis. J Biol Chem 1998;273:29066–71 [PubMed: 9786912]
10. Mao P, Hever MP, Niemaszyk LM, Haghkerdar JM, Yanco EG, Desai D, et al. Serine/threonine kinase 17A is a novel p53 target gene and modulator of cisplatin toxicity and reactive oxygen species in testicular cancer cells. J Biol Chem 2011;286:19381–91 [PubMed: 21489989]
11. Wittig R, Nessling M, Will RD, Mollenhauer J, Salowsky R, Munstermann E, et al. Candidate genes for cross-resistance against DNA-damaging drugs. Cancer Res 2002;62:6698–705 [PubMed: 12438269]
12. Guo Q, Chen Y, Wu Y. Enhancing apoptosis and overcoming resistance of gemcitabine in pancreatic cancer with bortezomib: a role of death-associated protein kinase-related apoptosis-inducing protein kinase 1. Tumori 2009;95:796–803 [PubMed: 20210246]
13. Gao J, Liu D, Li J, Song Q, Wang Q. Effect of STK17A on the sensitivity of ovarian cancer cells to paclitaxel and carboplatin. Oncol Lett 2016;12:1107–12 [PubMed: 27446402]
14. Mao P, Hever-Jardine MP, Rahme GJ, Yang E, Tam J, Kodali A, et al. Serine/threonine kinase 17A is a novel candidate for therapeutic targeting in glioblastoma. PLoS One 2013;8:e81803 [PubMed: 24312360]
15. Williams CS, Zhang B, Smith JJ, Jayagopal A, Barrett CW, Pino C, et al. BVES regulates EMT in human corneal and colon cancer cells and is silenced via promoter methylation in human colorectal carcinoma. J Clin Invest 2011;121:4056–69 [PubMed: 21911938]
16. Smith JJ, Deane NG, Wu F, Merchant NB, Zhang B, Jiang A, et al. Experimentally derived metastasis gene expression profile predicts recurrence and death in patients with colon cancer. Gastroenterology 2010;138:958–68 [PubMed: 19914252]
17. The Cancer Genome Atlas N. Comprehensive molecular characterization of human colon and rectal cancer. Nature 2012;487:330 [PubMed: 22810696]
18. Marisa L, de Reynies A, Duval A, Selves J, Gaub MP, Vescovo L, et al. Gene expression classification of colon cancer into molecular subtypes: characterization, validation, and prognostic value. PLoS Med 2013;10:e1001453 [PubMed: 23700391]
19. Barretina J, Caponigro G, Stransky N, Venkatesan K, Margolin AA, Kim S, et al. The Cancer Cell Line Encyclopedia enables predictive modelling of anticancer drug sensitivity. Nature 2012;483:603–7 [PubMed: 22460905]
20. Carpenter AE, Jones TR, Lamprecht MR, Clarke C, Kang IH, Friman O, et al. CellProfiler: image analysis software for identifying and quantifying cell phenotypes. Genome Biol 2006;7:R100 [PubMed: 17076895]
21. Sato T, Stange DE, Ferrante M, Vries RG, Van Es JH, Van den Brink S, et al. Long-term expansion of epithelial organoids from human colon, adenoma, adenocarcinoma, and Barrett's epithelium. Gastroenterology 2011;141:1762–72 [PubMed: 21889923]
22. Ashby WJ, Wikswo JP, Zijlstra A. Magnetically attachable stencils and the non-destructive analysis of the contribution made by the underlying matrix to cell migration. Biomaterials 2012;33:8189–203 [PubMed: 22940214]
23. Heijmans J, van Lidth de Jeude JF, Koo BK, Rosekrans SL, Wielenga MC, van de Wetering M, et al. ER stress causes rapid loss of intestinal epithelial stemness through activation of the unfolded protein response. Cell Rep 2013;3:1128–39 [PubMed: 23545496]
24. Du F, Zhao X, Fan D. Soft Agar Colony Formation Assay as a Hallmark of Carcinogenesis. Bio-protocol 2017;7:e2351
25. Zhao XD, Lu YY, Guo H, Xie HH, He LJ, Shen GF, et al. MicroRNA-7/NF-kappaB signaling regulatory feedback circuit regulates gastric carcinogenesis. J Cell Biol 2015;210:613–27 [PubMed: 26261179]

26. Leibovitz A, Stinson JC, McCombs WB 3rd, McCoy CE, Mazur KC, Mabry ND. Classification of human colorectal adenocarcinoma cell lines. Cancer Res 1976;36:4562–9 [PubMed: 1000501]
27. Brattain MG, Fine WD, Khaled FM, Thompson J, Brattain DE. Heterogeneity of malignant cells from a human colonic carcinoma. Cancer Res 1981;41:1751–6 [PubMed: 7214343]
28. Desai R, Sarpal R, Ishiyama N, Pellikka M, Ikura M, Tepass U. Monomeric alpha-catenin links cadherin to the actin cytoskeleton. Nat Cell Biol 2013;15:261–73 [PubMed: 23417122]
29. Lamouille S, Xu J, Derynck R. Molecular mechanisms of epithelial-mesenchymal transition. Nat Rev Mol Cell Biol 2014;15:178–96 [PubMed: 24556840]
30. Hay ED. The mesenchymal cell, its role in the embryo, and the remarkable signaling mechanisms that create it. Dev Dyn 2005;233:706–20 [PubMed: 15937929]
31. Voulgari A, Pintzas A. Epithelial-mesenchymal transition in cancer metastasis: mechanisms, markers and strategies to overcome drug resistance in the clinic. Biochim Biophys Acta 2009;1796:75–90 [PubMed: 19306912]
32. Coleman ML, Sahai EA, Yeo M, Bosch M, Dewar A, Olson MF. Membrane blebbing during apoptosis results from caspase-mediated activation of ROCK I. Nat Cell Biol 2001;3:339–45 [PubMed: 11283606]
33. Vicente-Manzanares M, Ma X, Adelstein RS, Horwitz AR. Non-muscle myosin II takes centre stage in cell adhesion and migration. Nat Rev Mol Cell Biol 2009;10:778–90 [PubMed: 19851336]
34. Hagmann J, Burger MM, Dagan D. Regulation of plasma membrane blebbing by the cytoskeleton. J Cell Biochem 1999;73:488–99 [PubMed: 10733343]
35. Kovacs M, Toth J, Hetenyi C, Malnasi-Csizmadia A, Sellers JR. Mechanism of blebbistatin inhibition of myosin II. J Biol Chem 2004;279:35557–63 [PubMed: 15205456]
36. Wilkinson S, Paterson HF, Marshall CJ. Cdc42-MRCK and Rho-ROCK signalling cooperate in myosin phosphorylation and cell invasion. Nat Cell Biol 2005;7:255–61 [PubMed: 15723050]
37. Short SP, Costacurta PW, Williams CS. Using 3D Organoid Cultures to Model Intestinal Physiology and Colorectal Cancer. Curr Colorectal Cancer Rep 2017;13:183–91 [PubMed: 29276469]
38. Wakatsuki T, Wysolmerski RB, Elson EL. Mechanics of cell spreading: role of myosin II. J Cell Sci 2003;116:1617–25 [PubMed: 12640045]
39. Tang H, Liu YJ, Liu M, Li X. Establishment and gene analysis of an oxaliplatin-resistant colon cancer cell line THC8307/L-OHP. Anticancer Drugs 2007;18:633–9 [PubMed: 17762391]
40. Kerley-Hamilton JS, Pike AM, Li N, DiRenzo J, Spinella MJ. A p53-dominant transcriptional response to cisplatin in testicular germ cell tumor-derived human embryonal carcinoma. Oncogene 2005;24:6090–100 [PubMed: 15940259]
41. Oue Y, Murakami S, Isshiki K, Tsuji A, Yuasa K. Intracellular localization and binding partners of death associated protein kinase-related apoptosis-inducing protein kinase 1. Biochem Biophys Res Commun 2018;496:1222–8 [PubMed: 29397938]
42. Thomas A, Mahantshetty U, Kannan S, Deodhar K, Shrivastava SK, Kumar-Sinha C, et al. Expression profiling of cervical cancers in Indian women at different stages to identify gene signatures during progression of the disease. Cancer Med 2013;2:836–48 [PubMed: 24403257]
43. Nowell CS, Radtke F. Notch as a tumour suppressor. Nat Rev Cancer 2017;17:145–59 [PubMed: 28154375]
44. Park Y, Kim W, Lee JM, Park J, Cho JK, Pang K, et al. Cytoplasmic DRAK1 overexpressed in head and neck cancers inhibits TGF-beta1 tumor suppressor activity by binding to Smad3 to interrupt its complex formation with Smad4. Oncogene 2015;34:5037–45 [PubMed: 25531329]
45. Yang KM, Kim W, Bae E, Gim J, Weist BM, Jung Y, et al. DRAK2 participates in a negative feedback loop to control TGF-beta/Smads signaling by binding to type I TGF-beta receptor. Cell Rep 2012;2:1286–99 [PubMed: 23122956]
46. Padua D, Massague J. Roles of TGFbeta in metastasis. Cell Res 2009;19:89–102 [PubMed: 19050696]
47. Markowitz SD, Roberts AB. Tumor suppressor activity of the TGF-beta pathway in human cancers. Cytokine Growth Factor Rev 1996;7:93–102 [PubMed: 8864357]

48. Bellam N, Pasche B. Tgf-beta signaling alterations and colon cancer. Cancer Treat Res 2010;155:85–103 [PubMed: 20517689]
49. Ilyas M, Efstathiou JA, Straub J, Kim HC, Bodmer WF. Transforming growth factor beta stimulation of colorectal cancer cell lines: type II receptor bypass and changes in adhesion molecule expression. Proc Natl Acad Sci U S A 1999;96:3087–91 [PubMed: 10077641]
50. Woodford-Richens KL, Rowan AJ, Gorman P, Halford S, Bicknell DC, Wasan HS, et al. SMAD4 mutations in colorectal cancer probably occur before chromosomal instability, but after divergence of the microsatellite instability pathway. Proc Natl Acad Sci U S A 2001;98:9719–23 [PubMed: 11481457]
51. Harris TL, McGargill MA. Drak2 Does Not Regulate TGF-beta Signaling in T Cells. PLoS One 2015;10:e0123650 [PubMed: 25951457]
52. Gilmore AP. Anoikis. Cell Death Differ 2005;12 Suppl 2:1473–7 [PubMed: 16247493]
53. Chen G, Hou Z, Gulbranson DR, Thomson JA. Actin-myosin contractility is responsible for the reduced viability of dissociated human embryonic stem cells. Cell Stem Cell 2010;7:240–8 [PubMed: 20682449]

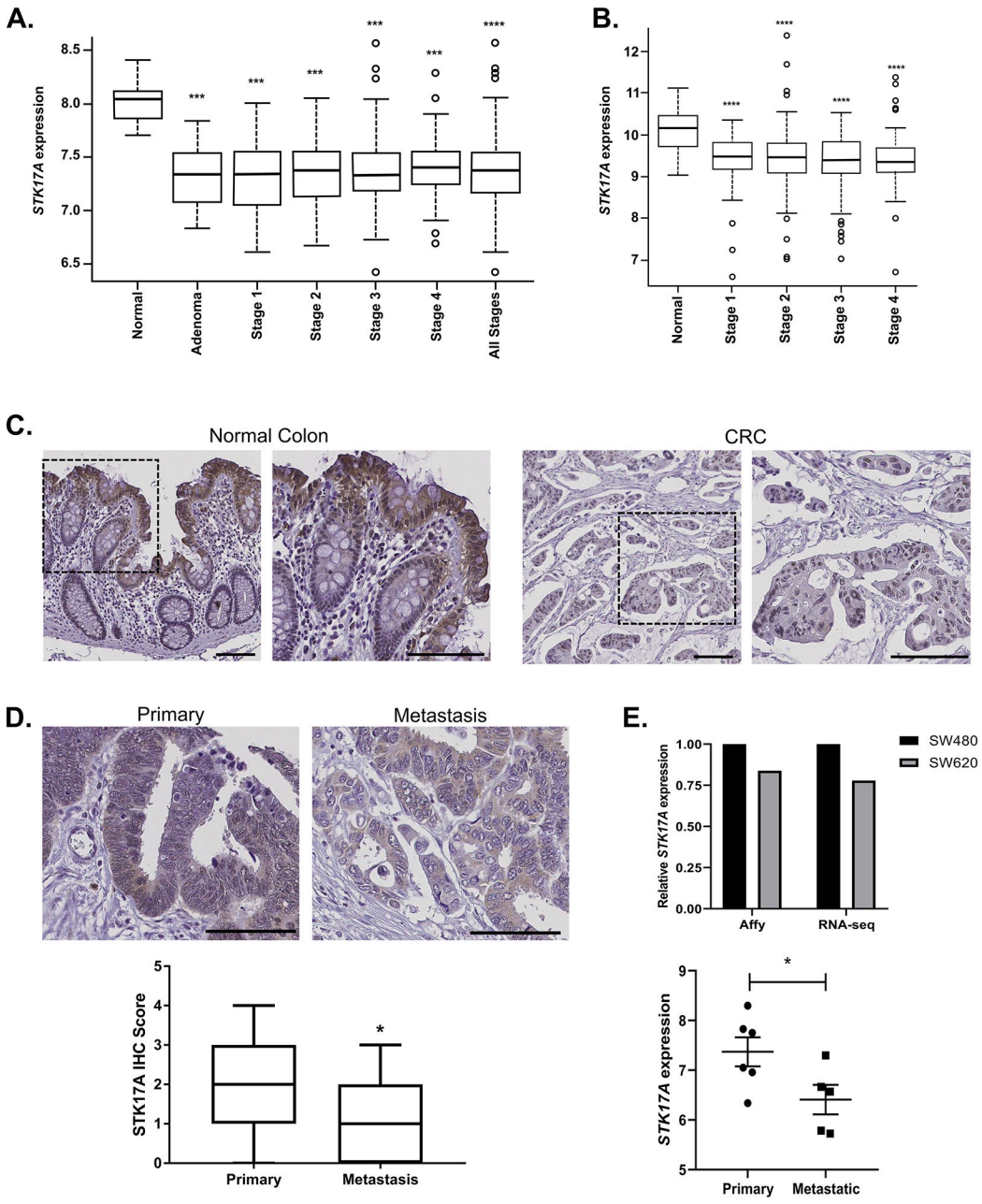

Figure 1. STK17A is decreased in colorectal tumors and metastases.

A. *STK17A* expression was queried from a joint Moffitt Cancer Center/Vanderbilt Medical Center microarray of normal colon (n=10), colon adenomas (n=6), and colorectal cancer samples (n=250). **B.** *STK17A* expression was queried from The Cancer Genome Atlas colon adenocarcinoma data set and normalized RSEM expression data were log2 transformed for visualization. Average values for *STK17A* in normal colon (n = 39) and colorectal tumors (CRC; n = 264) divided by stage. **C.** Representative images of immunohistochemistry for STK17A in normal colon (left) and stage 4 colorectal cancer (CRC, right). Dotted line denotes inset area. **D.** Representative STK17A staining of a matched primary and metastatic tumor from a curated tissue CRC/metastasis microarray (top) and quantification of staining

intensity assessed by a blinded observer and assigned a 0-4 score (bottom, n=58 primary and 30 metastatic tumors). **E.** *STK17A* expression in SW480 and SW620 cells was queried from an Affymetrix array and RNA-sequencing expression datasets in the Broad Institute Cancer Cell Line Encyclopedia (top). For each dataset, levels observed in SW480 cells was normalized to 1. *STK17A* expression in the Affymetrix array dataset for primary-derived colon cancer cell lines (SW480, HCT116, Caco-2, DLD1, RKO, HCT-8) as compared to metastatic-derived colon cancer cell lines (SW620, COLO 205, COLO 201, LoVo, SNU-C1) (bottom). Scale bars = 50μm. *P<0.05, ***P<0.001, ****P<0.0001, Wilcoxon rank sum test with continuity correction (A and B) or Student's t test (D and E).

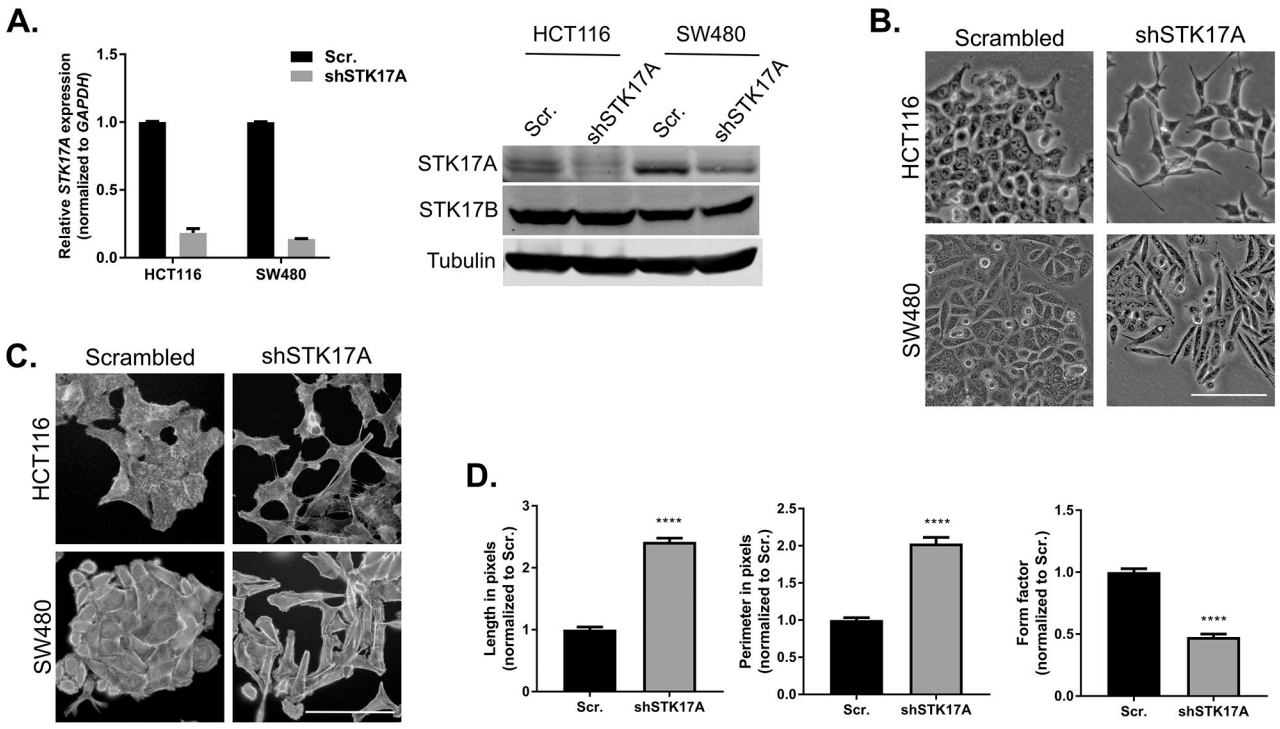

Figure 2. Loss of STK17A induces mesenchymal morphology in CRC cells.

A. Analysis of *STK17A* expression in knockdown (shSTK17A) vs. control cells (Scr.) assessed by qPCR (left) and western blot (right) in HCT116 and SW480 CRC cells, along with family member STK17B. **B.** Brightfield images of shSTK17A cells in HCT116 and SW480 cells. **C.** Scrambled and shSTK17A cells were plated on coverslips and stained for actin to analyze cell shape. **D.** Morphometric analysis by CellProfiler to assess length (left), perimeter (middle), and form factor (right). All measurements were normalized to scrambled shRNA control cells (n=20 cells per analysis). Scale bars = 50μm. ****$P<0.0001$, Student's t test. Error bars ± SEM.

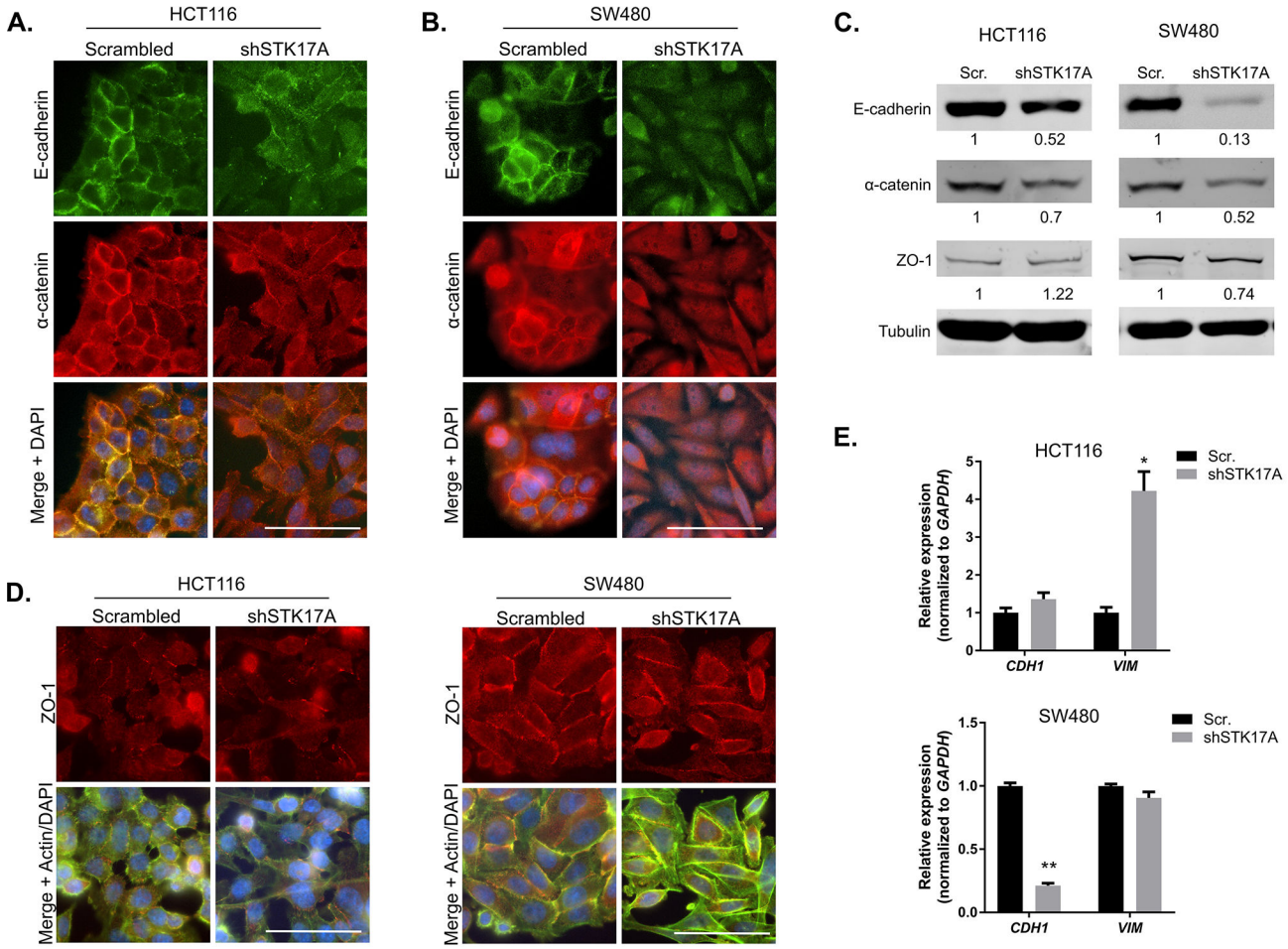

Figure 3. *STK17A* knockdown decreases expression of adherens junction proteins.

A. Representative immunofluorescent staining for E-cadherin (green) and α-catenin (red) in HCT116 and **B.** SW480 cells. **C.** Western blot analysis of E-cadherin, α-catenin, and ZO-1 in HCT116 (left) and SW480 (right) cells. Tubulin was used as a loading control. Numbers below bands indicate protein levels normalized to tubulin and represented as fold change over scrambled shRNA control cells (Scr.), representative of 3 independent experiments. **D.** Staining for ZO-1 (red) merged with DAPI (blue) and actin (green) in HCT116 cells (left) and SW480 cells (right). **E.** qPCR analysis for expression of E-cadherin (*CDH1*) and Vimentin (*VIM*). Scale bars = 50μm. **P*<0.05, ***P*<0.01, Student's t test. Error bars ± SEM.

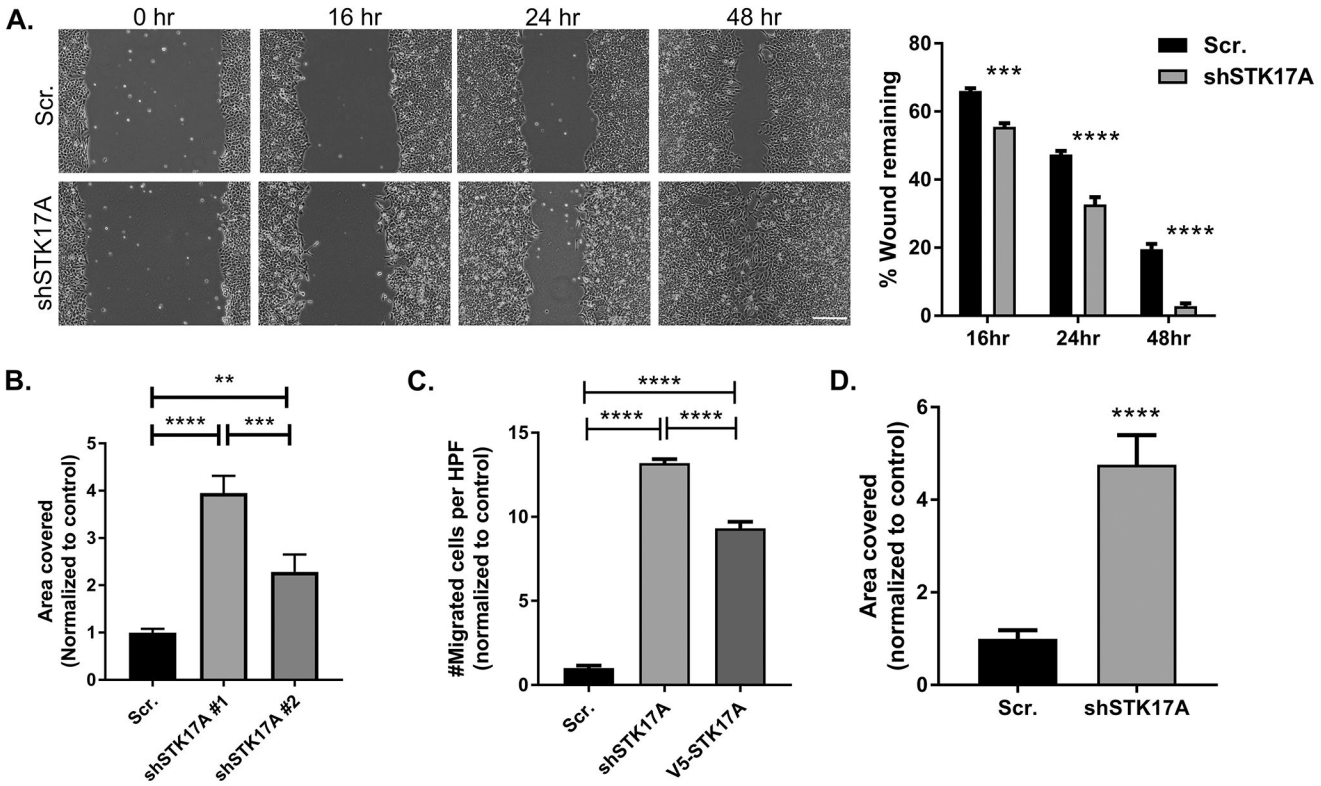

Figure 4. *STK17A* knockdown augments migration and invasion in CRC cells.

A. HCT116 cell migration assessed by MAts assay. Images were captured at 0, 16, 24, and 48 hours post stencil removal (left) and wound width was measured using ImageJ to calculate the percent distance remaining at each timepoint (right). Representative of 4 independent experiments. **B.** Scrambled shRNA (Scr.), shSTK17A #1, and shSTK17A #2 cells were plated in transwell inserts and allowed to migrate for 72 hours. Afterward, cells were fixed, stained, imaged, and the area of each high-powered field covered by migrated cells was quantified in ImageJ. n=5 images per insert, 3 inserts per condition, combined data of 3 independent experiments **C.** Scrambled shRNA (Scr.), shSTK17A, and shSTK17A cells transiently expressing a V5-tagged STK17A (V5-STK17A) were plated in transwell inserts and allowed to migrate for 72 hours. Afterward, cells were fixed, stained, imaged, and counted in each high-powered field. n=5 images per insert, 3 inserts per condition, representative of 3 independent experiments. **D.** Scrambled shRNA (Scr.) and shSTK17A cells were plated in Matrigel coated transwell inserts and allowed to migrate for 72 hours. Migrated cells were imaged and the cell-containing area quantified by ImageJ and standardized to Scr. n=5 images per insert, 3 inserts per condition, representative data from 3 independent experiments. Scale bars = 100μm. ** $P<0.01$, *** $P<0.001$, **** $P<0.0001$, Student's t test (A & D) or one-way ANOVA with Tukey's multiple comparisons test (B & C). Error bars ± SEM.

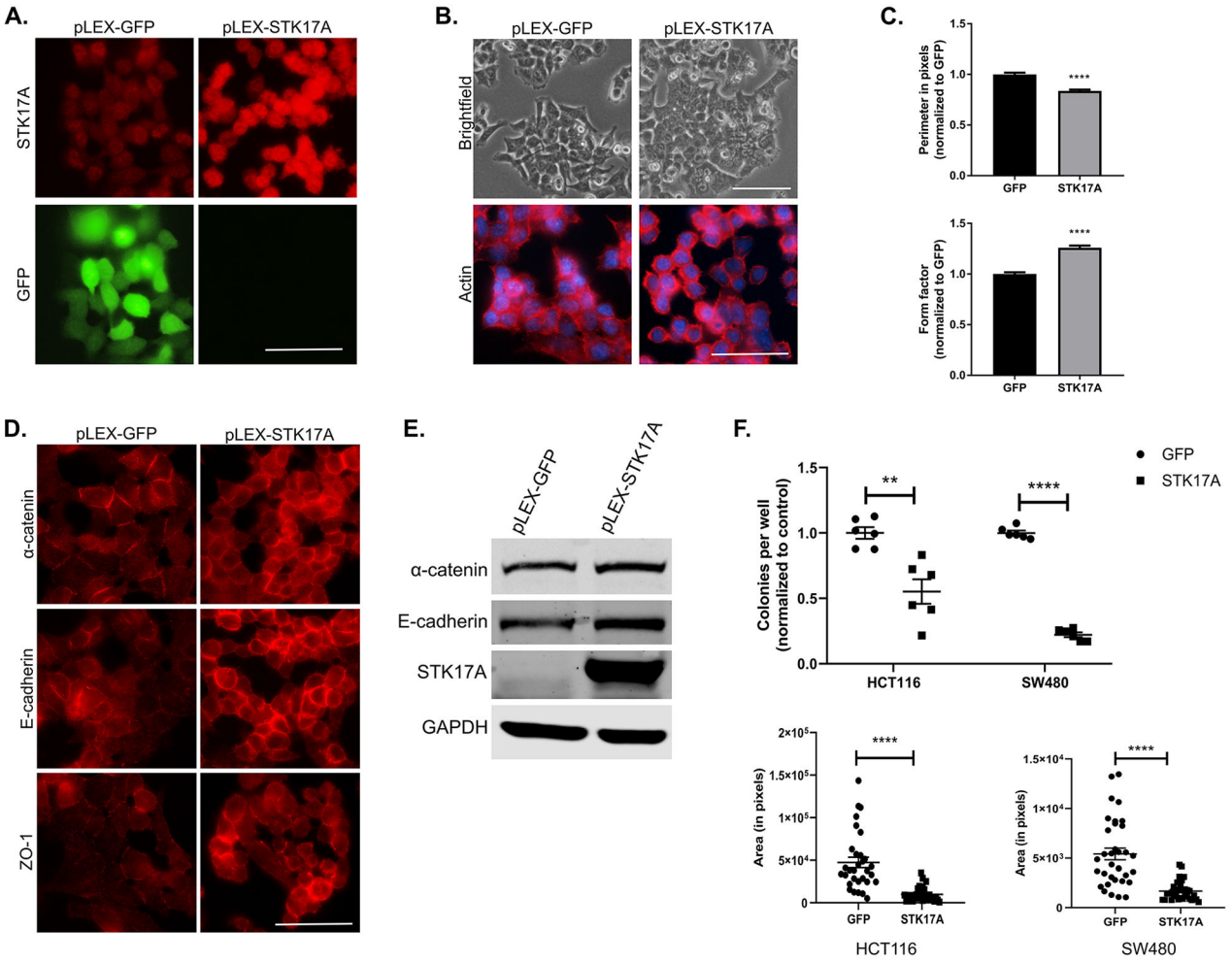

Figure 5. STK17A overexpression attenuates mesenchymal phenotypes.

A. Staining for STK17A (red) and GFP (green) in HCT116 cells expressing either the pLEX-STK17A or pLEX-GFP control vector. **B.** Analysis of cell morphology by brightfield microscopy (top) or ActinRed staining (bottom). **C.** Morphometric analysis by CellProfiler to assess perimeter (top), and form factor (bottom). All measurements were normalized to pLEX-GFP control cells. n=100 cells per analysis. **D.** Immunofluorescent staining for α-catenin, E-cadherin, and ZO-1 in pLEX-GFP (top) and pLEX-STK17A (bottom) cells. **E.** Analysis of α-catenin, E-cadherin, and STK17A by western blot. GAPDH was used as a loading control. **F.** Colony number (top) and colony size (bottom) of pLEX-GFP and pLEX-STK17A HCT116 and SW480 cells 10 days post-plating in soft agar. n=3 wells per experiment, combined data from 2 independent experiments. For area measurements 5-7 colonies were measured per well and quantified (in pixels) by ImageJ software. Scale bars = 50μm. ** P<0.01, **** P<0.0001, Student's t test. Error bars ± SEM.

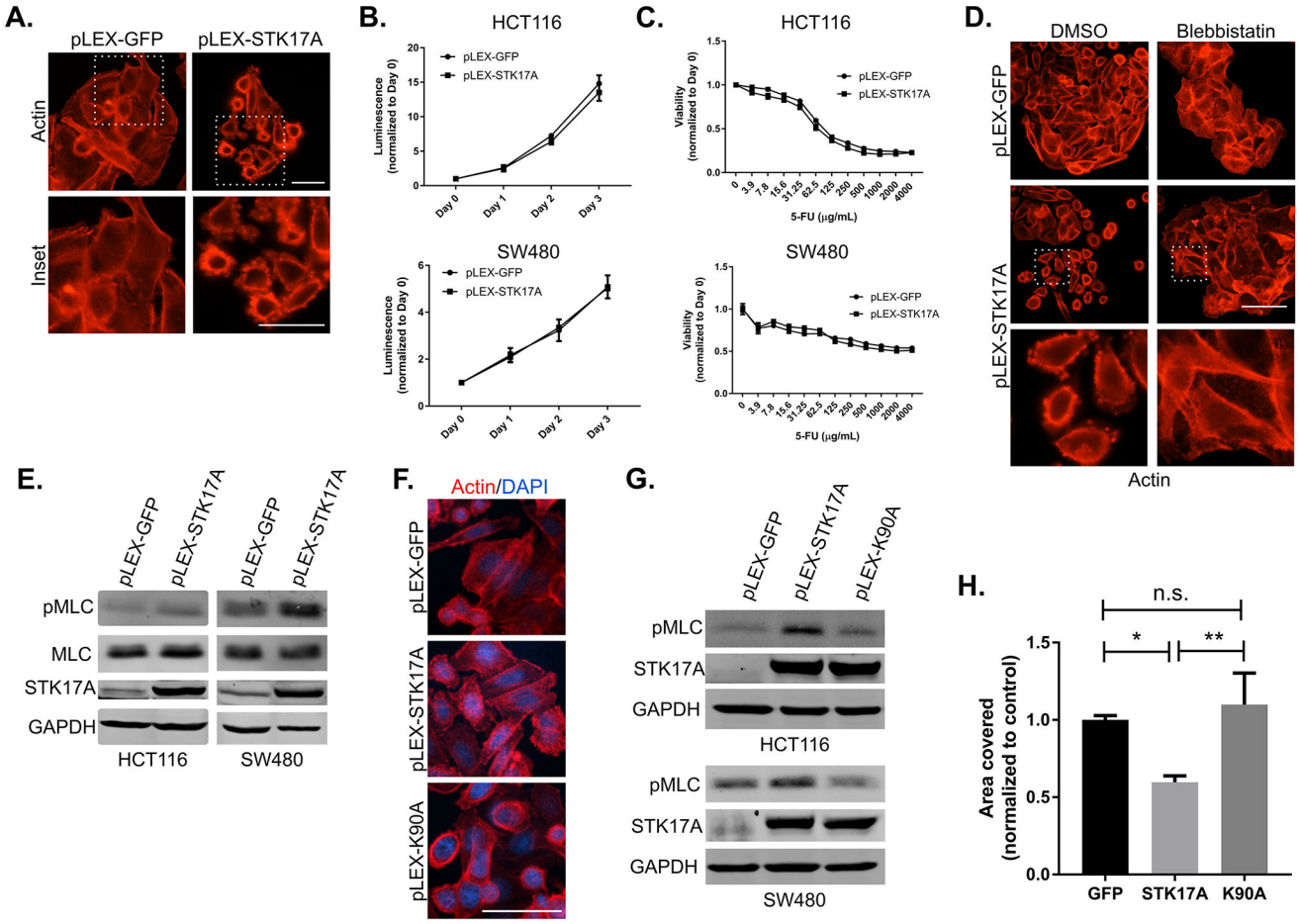

Figure 6. Overexpression of STK17A induced cell contractility without affecting apoptosis.

A. Membrane blebbing apparent in pLEX-STK17A SW480 cells via staining with ActinRed. Dotted line denotes inset area. Scale bar = 25μm. **B.** Growth curves of HCT116 (top) and SW480 (bottom) pLEX-GFP control and pLEX-STK17A expressing cells. Viable cells were measured daily via CellTiter Glo reagent. n=3 wells per experiment, combined data from 3 independent experiments. **C.** HCT116 (top) and SW480 (bottom) cells were treated with 5-FU at the concentrations described for 72 hours. Cell viability was measured by CellTiter Blue and normalized to pre-5-FU viability measurements. n=3 wells per experiment, combined data from 3 independent experiments. **D.** SW480 lines were treated with DMSO (top) or 100μM blebbistatin for 2 hours prior to fixing and imaging with ActinRed. Dotted line denotes inset area. Scale bar = 50μm. **E.** Western blot analysis for phosphorylated myosin light chain (pMLC), total myosin light chain (MLC), and STK17A in HCT116 (left) and SW480 cells (right). GAPDH was used as a loading control. **F.** Extended depth of field images of actin (red) and DAPI (blue) staining in pLEX-GFP, pLEX-STK17A, and pLEX-K90A SW480 cells. Scale bar = 25μm. **G.** Western blot analysis for phosphorylated myosin light chain (pMLC), total myosin light chain (MLC), and STK17A in HCT116 (left) and SW480 cells (right) with pLEX-GFP, pLEX-STK17A, or pLEX-K90A (kinase-dead STK17A) expression. GAPDH was used as a loading control. Representative of 3 independent experiments. **H.** pLEX-GFP, pLEX-STK17A, or pLEX-

K90A (kinase-dead STK17A) expressing cells were plated on transwell inserts. After 72 hours cells were fixed, imaged, and the cell-containing area was quantified by ImageJ and standardized to control cell readings. n=3 wells per experiment, combined data from 3 independent experiments. *P<0.05, **P<0.01, one-way ANOVA with Tukey's multiple comparisons test. n.s. = nonsignificant. Error bars ± SEM.

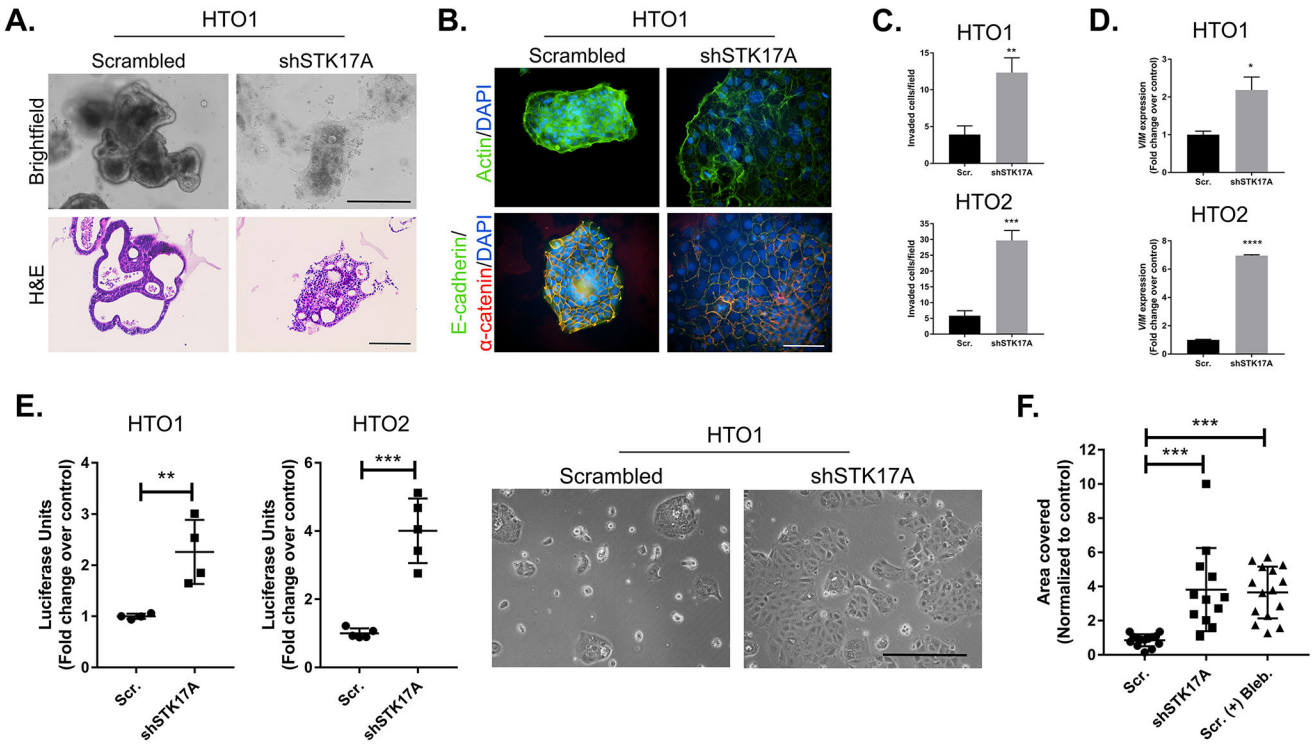

Figure 7. STK17A maintains epithelial phenotypes in primary human tumor organoids.

A. Altered morphology in HTO1 assessed by brightfield microscopy (top) and H&E staining (bottom). Scale bar = 100μm. **B.** Cells from the HTO1 line were dissociated and plated on glass coverslips coated with a thin layer of 50/50 Matrigel and human organoid media. After adherence, cells were fixed and stained for actin (green, top) or E-cadherin (green) and α-catenin (red, bottom). Overlays for each stain shown with DAPI (blue). Scale bar = 50μm. **C.** HTO cells were dissociated and plated in Matrigel-coated transwell inserts and allowed to migrate for 96 hours. The number of invaded cells was calculated per 10X field. n=12 fields, representative of 2 independent experiments. **D.** qPCR analysis of vimentin (*VIM*) expression in HTO1 (top) and HTO2 (bottom) lines. **E.** Cells from HTO1 and HTO1 lines were dissociated and plated in uncoated tissue culture plates. After 96 hours, cells from HTO1 (left) and HTO2 (middle) were analyzed by CellTiter Glo and normalized to scrambled shRNA control lines (left). n=2-3 wells per experiment, combined data from 2 independent experiments. Representative brightfield images of HTO1 (right). Scale bar = 100μm. **F.** Cells from HTO1 lines were dissociated and plated on plastic with DMSO or 50μM blebbistatin. Cell-covered area was measured after 48 hours and normalized to amount observed in control cells. n=2-5 images per well, 2-3 wells per experiment, combined data from 3 independent experiments. *P<0.05, **P<0.01, ***P<0.001, ****P<0.0001, Student's t test (C, D, E) or one-way ANOVA with Tukey's multiple comparisons test (F). Error bars ± SEM.